ISSN 2072-5981
doi: 10.26907/mrsej

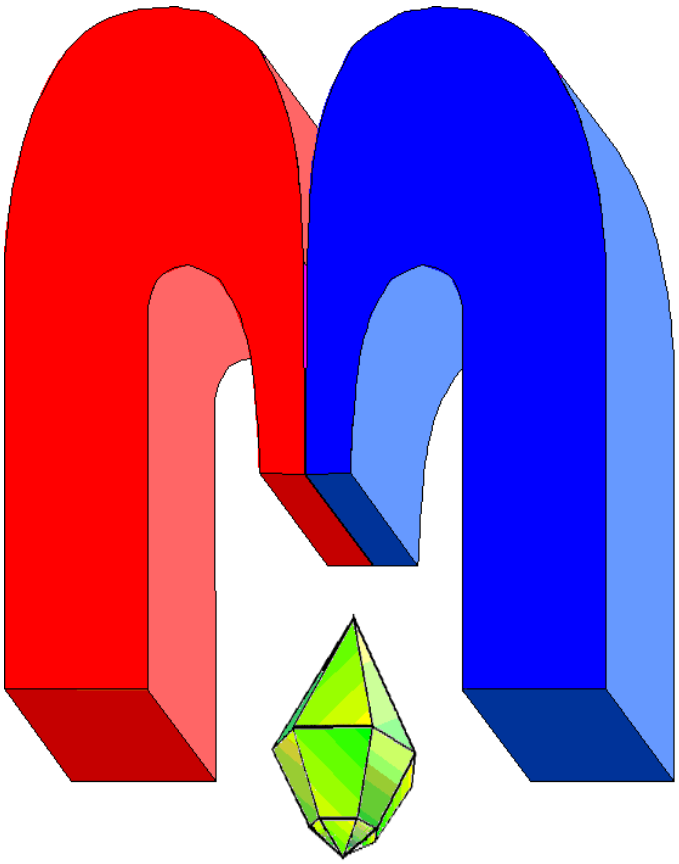

Magnetic Resonance in Solids

Electronic Journal

Volume ***21***
Special Issue ***4***
Paper No ***19406***
1-11 pages
2019
doi: **10.26907/mrsej-19406**

http://mrsej.kpfu.ru
http://mrsej.ksu.ru

Established and published by Kazan University
Endorsed by International Society of Magnetic Resonance (ISMAR)
Registered by Russian Federation Committee on Press (#015140), August 2, 1996
First Issue appeared on July 25, 1997

"***Magnetic Resonance in Solids. Electronic Journal***" (**MRS*ej***) is a peer-reviewed, all electronic journal, publishing articles which meet the highest standards of scientific quality in the field of basic research of a magnetic resonance in solids and related phenomena.

Indexed and abstracted by
Web of Science (*ESCI*, Clarivate Analytics, from 2015), *Scopus* (Elsevier, from 2012), *RusIndexSC* (*eLibrary*, from 2006), *Google Scholar*, *DOAJ*, *ROAD*, *CyberLeninka* (from 2006), *SCImago Journal & Country Rank*, etc.

* In Kazan University the Electron Paramagnetic Resonance (EPR) was discovered by Zavoisky E.K. in 1944.

Short cite this: *Magn. Reson. Solids* **21**, 19406 (2019) doi: 10.26907/mrsej-19406

Phonon spectrum of $Nd_2Zr_2O_7$ crystal: *ab initio* calculation

V.A. Chernyshev

Ural Federal University, Mira 19, Ekaterinburg 620002, Russia

E-mail: vladimir.chernyshev@urfu.ru

(Received May 25, 2019; accepted May 28, 2019; published June 6, 2019)

Crystal structure and phonon spectrum of rare-earth pyroclore oxide $Nd_2Zr_2O_7$ were studied within the framework of density functional theory and MO LKAO approach. The calculations were performed by using hybrid functionals that take into account both local and nonlocal (at the Hartree-Fock formalism) exchanges. Calculations were performed with the functionals PBESOL0 and PBE0. The fundamental vibration frequencies of $Nd_2Zr_2O_7$ were calculated. The calculations were performed in the CRYSTAL17 program designed to simulate periodic structures.

PACS: 61.50.Ah, 63.20.dk.
Keywords: phonon spectrum, DFT, hybrid functionals, pyrochlores.

Dedicated to Boris Malkin, on the occasion of his 80th birthday

1. Introduction

The growing interest to the study of neodymium zirconate $Nd_2Zr_2O_7$ has to do with varies of their properties and applications [1–3]. The crystal field on the rare-earth ion at pyrochlore structure have been studied at [4, 5]. Neodymium zirconate $Nd_2Zr_2O_7$ was experimentally investigated by methods of X-ray diffraction, Raman and IR spectroscopy [6–16]. The structural phase transformation from fluorite to pyrochlore phase was studied by Raman spectroscopy [10]. However, not all the phonon modes corresponding to the pyrochlore structure were detected during the experiments. Most of the measurements were carried out on polycrystals. Therefore, it is relevant to perform *ab initio* calculation of the phonon spectrum, which will determine the frequencies and types of the phonon modes for pyrochlore structures of $Nd_2Zr_2O_7$. In this work, the phonon spectrum of the crystal $Nd_2Zr_2O_7$ with the pyrochlore structure ($Fd\bar{3}m$) is investigated in the framework of the MO LCAO approach with hybrid DFT functionals.

2. Calculations

Ab initio calculations were performed within the framework of the density functional theory (DFT) by using hybrid functionals which take into account both local and non-local (in the Hartree-Fock formalism) exchange. Calculations were performed with PBE0 [17] functional, as well as PBESOL0 functional, which is incremented in the program CRYSTAL17 [18, 19]. The percentage of HF-exchange at PBESOL0 functional is 25% as well as in PBE0. By using the hybrid functionals that take into account both local and non-local (HF) exchanges, we can well describe the band structure, IR and Raman spectra, and elastic properties of compounds with an ion-covalent bond [20]. Comparison of PBE0 and other functionals with CCSD calculations has been performed recently (128 functionals of different levels were tested) [21]. It was shown that PBE0 is characterized by a rather small error for functionals of its level relative to the CCSD calculation when reproducing electron density and other parameters [21]. By using the PBE0 hybrid functional, we successfully described the structure and dynamics of the crystal lattice of rare-earth titanates with the pyrochlore structure $R_2Ti_2O_7$ (R – rare-earth ion) in our previous work [22]. Oxygen is part of all structural units in the pyrochlore structure. It is located in two symmetrically nonequivalent positions (Table 1). Therefore, the reproduction of the structure and properties will depend essentially on the oxygen basis. The basis of TZVP type was used in work [23]. This basis is available on CRYSTAL website [24]. Zirconium

basis [25] is available on CRYSTAL website also. This basis was used by the authors of the CRYSTAL program to calculate the structure and IR spectrum of zirconium complexes with oxygen ligands [25]. Quasi-relativistic pseudopotential ECP*49*MWB was used to describe the inner shells of the neodymium (ECP – "effective core potential"; 49 is the number of internal electrons replaced by a pseudopotential; WB is "quasi-relativistic") [26, 27]. Accordingly, the inner shells of the rare-earth ion were replaced by a pseudopotential on the $4f$ inclusive. TZVP type valence basis sets "ECP*49*MWB-II" were used to describe the outer shells, $5s^25p^6$, involved in the formation of chemical bonds [26, 28, 29]. These pseudopotential and valence basis sets are available on the Stuttgart website [30]. Gaussian primitives with exponent values less than 0.1 were removed from the valence basis sets. The last diffuse orbital of the f type was also removed from the valence basis sets. The sequence of calculations was the following. Firstly, the optimization of the crystal structure was carried out. After that, the phonon spectrum (or the elastic constants) was calculated for the crystal structure corresponding to the minimum energy. The solving accuracy of self-consistent system of Kohn-Sham equations was set at 10^{-10} a.u. (TOLDEE = 10). The parameters "TOLINTEG", determining the accuracy of the calculation of the two-electron integrals were set equal to $8, 8, 8, 8, 16$. The Monkhorst-Pack shrinking factor was taken to be 8. The phonon spectrum in the CRYSTAL program was calculated at the harmonic approximation. When calculating the Hessian matrix, the first derivatives were calculated analytically, while the second derivatives were calculated numerically. The Born charges were used by calculations of the Raman and infrared intensities at CRYSTAL code [31]. Electric dipole properties were calculated by using a periodic Coupled-perturbed Hartree-Fock (CPHF) or Kohn-Sham (CPKS) approach [32–34]. Details of the calculation algorithms are presented in [35]. The Placzek approximation was used to calculate the intensity of the Raman modes [33]. Non-resonant Raman intensities were calculated as well. According to [18, 24, 35], the mode intensity associated to an oriented single crystal is:

$$I_{ij}^k \propto C(\alpha_{ij}^k)^2. \tag{1}$$

Here $i, j = x, y, z$, and α_{ij}^k is the element of the Raman tensor. The latter is given by

$$\alpha_{ij}^k = \frac{\partial^3 E^{\mathrm{TOT}}}{\partial Q_k \partial \varepsilon_i \varepsilon_j}. \tag{2}$$

The element α_{ij}^k is calculated as the third derivative of the total electron energy. Here Q_k is the normal mode coordinate, $\boldsymbol{\varepsilon}$ is the external electric field. The value C defined by the laser frequency ω_L and temperature T is as follows:

$$C \backsim \frac{1 + n(\omega_k)}{30\,\omega_k}(\omega_L - \omega_k)^4. \tag{3}$$

Taking into account the Bose occupancy factor $n(\omega_k)$, we obtain

$$1 + n(\omega_k) = \left[1 - \exp\left(-\frac{\hbar\,\omega_k}{k_{\mathrm{B}}T}\right)\right]^{-1}. \tag{4}$$

For a powder polycrystalline sample, the integral intensity is averaged over the possible directions of an ideal bulk crystal [36]. The rotational invariants $G_k^{(n)}$ are defined as:

$$G_k^{(0)} = \frac{1}{3}\left(\alpha_{xx}^k + \alpha_{yy}^k + \alpha_{zz}^k\right)^2, \tag{5}$$

$$G_k^{(1)} = \frac{1}{2}\left[\left(\alpha_{xy}^k - \alpha_{yx}^k\right)^2 + \left(\alpha_{xz}^k - \alpha_{zx}^k\right)^2 + \left(\alpha_{zy}^k - \alpha_{yz}^k\right)^2\right], \tag{6}$$

$$G_k^{(2)} = \frac{1}{2}\left[\left(\alpha_{xy}^k + \alpha_{yx}^k\right)^2 + \left(\alpha_{xz}^k + \alpha_{zx}^k\right)^2 + \left(\alpha_{zy}^k + \alpha_{yz}^k\right)^2\right] + \\ + \frac{1}{3}\left[\left(\alpha_{xx}^k - \alpha_{yy}^k\right)^2 + \left(\alpha_{xx}^k - \alpha_{zz}^k\right)^2 + \left(\alpha_{yy}^k - \alpha_{zz}^k\right)^2\right]. \quad (7)$$

The Raman intensities of the two polarized components of the powder spectra, the parallel and perpendicular ones, are

$$I_{\parallel,k}^{\text{powder}} = C\left(10G_k^{(0)} + 4G_k^{(2)}\right), \quad (8)$$

$$I_{\perp,k}^{\text{powder}} = C\left(5G_k^{(1)} + 3G_k^{(2)}\right), \quad (9)$$

$$I_{\text{tot},k}^{\text{powder}} = I_{\parallel,k}^{\text{powder}} + I_{\perp,k}^{\text{powder}}. \quad (10)$$

The C value in the terms (8), (9) is defined in Eq. (3). The infrared intensity of the p-th mode [18] is defined as

$$I_p = \frac{\pi}{3}\frac{N_A}{c^2} d_p \left|\mathbf{Z}_p\right|^2, \quad (11)$$

where N_A is Avogadro's number, c is the speed of light, d_p is the degeneracy of the mode, and $\mathbf{Z}_p$ is the mass-weighted effective-mode Born charge vector. The infrared intensity is calculated assuming an isotropic response.

3. Results and discussion

The coordinates of the ions in the unit cell of the crystal $Nd_2Zr_2O_7$ with the pyrochlore structure ($Fd\bar{3}m$) are given in Table 1.

The crystal structure of $Nd_2Zr_2O_7$ was calculated with PBE0 and PBESOL0 hybrid functionals. The results are shown in Table 2. The calculation results are in good agreement with the experimental data.

Rare-earth zirconate $Nd_2Zr_2O_7$ with pyrochlore structure has phonon modes at the Γ point: $\Gamma = A_{1g} + E_g + 2F_{1g} + 4F_{2g} + 3A_{2u} + 3E_u + 8F_{1u} + 4F_{2u}$. Here A_{1g}, E_g and $4F_{2g}$ are Raman active modes, $7F_{1u}$ are infrared active modes, $4F_{2u}$, $3E_u$, $2F_{1g}$, $3A_{2u}$ are silent modes. The results of the calculation of phonon modes at the Γ point of $Nd_2Zr_2O_7$ are given in Table 3. Frequencies and types of the phonon modes were determined from the *ab initio* calculation. From the analysis of displacement vectors obtained from this *ab initio* calculations, the degree of participation of each ion in a particular mode was estimated (Table 3, Fig. 1). The ions that are shifted significantly in the mode are listed in the column "Ion-participants" at Table 3. The "S" index is a strong shift ("Strong"), "W" is weak ("Weak"). The maximum displacement of ions reaches ~ 0.04 Å. If the displacement of the ion is less than 0.01, the ion is not mentioned in the column "Ion-participants". If the value of its displacement is close to 0.01, it is indicated by the index "W". The results of the calculation of the intensity of Raman and infrared modes are shown in Tables 3-6 and Figures 2-3. We can distinguish between the modes in which only oxygen ions are involved, such as the infrared active mode F_{1u} with a frequency of 234 cm^{-1}. O1 ions, located at $48f$ position, characterized by the x coordinate, participate mainly in this mode. O1 is also predominantly involved in the most intense Raman mode F_{2g} (309 cm^{-1}). Only O1 ions are involved in the Raman E_g mode (328 cm^{-1}). According to calculations, this is the second most intense mode in the Raman spectrum (Table 5, Fig. 2). Only O1 ions also participate in the Raman modes A_{1g}. O1 ions participate mainly at the high-frequency F_{2g} mode (711 cm^{-1}). Thus, the behavior of these modes gives information about the value of the

x coordinate of the oxygen O1 under external impact on the crystal. The oxygen O2, located at $8b$ position, mainly participates in F_{2g} modes with frequencies of 414 and 537 cm^{-1}. The oxygen O2 participates mainly at infrared F_{1u} mode (391 cm^{-1}). All ions are involved in IR active modes (F_{1u}), but their displacement values are different. Zirconium and both O1 and O2 oxygens are involved in the most intense F_{1u} mode with a frequency of 333 cm^{-1}, with O1 taking the most participation (Table 3). At the low-frequency F_{1u} mode (98 cm^{-1}), mostly neodymium is involved. Lanthanum and zirconium are substantially involved in silent modes. The calculation results are in satisfactory agreement with Raman experiments on the powder samples (Figure 4). According to the calculations, oxygen O1 is predominantly involved in the most intense Raman mode F_{2g} (309 cm^{-1}). This result agrees with the experimental data [11], where the Zr-O6 bending was presumed at this mode.

According to the calculations, only O1 and O2 oxygens participate at F_{2g} mode with frequency 414 cm^{-1}. The result agrees with the experimental data [10], where it was assumed that the O-Nd-O′ vibrations are present in this mode (Table 7). The results of the simulation of the IR spectrum are shown in Fig. 1. The presence of the peak near 500 cm^{-1} agrees well with the measured IR transmittance spectrum of $Nd_2Zr_2O_7$ [16]. It follows from the calculations that neodymium is involved in the modes with frequencies up to 250 cm^{-1}. Zirconium participates in modes with frequencies up to 400 cm^{-1}. Oxygen O2 participates in modes with frequencies up to 550 cm^{-1}, while oxygen O1($48f$) participates in all modes (Figure 1).

The results of the calculation of the elastic constants and the bulk modulus are given in Tables 8-10. The results are in good agreement with the experimental data [13]. The mechanical stability criterion [37] (Born stability criterion) is performed for $Nd_2Zr_2O_7$.

Table 1. Ion coordinates in the $R_2Zr_2O_7$ unit cell.

Ion	x	y	z	Wyckoff position
Zr	0	0	0	16 c
Nd	1/2	1/2	1/2	16 d
O1	x	1/8	1/8	48 f
O2	3/8	3/8	3/8	8 b

Table 2. The lattice constant, interionic distances (Å), x coordinate of oxygen O1 (relative units) of the $Nd_2Zr_2O_7$ crystal.

	Calc. PBESOL0	Calc. PBE0	Exp. [9]	Exp. [1]	Exp. [13]	Exp. [5]	Exp. [15]
Lattice constant	10.6526	10.7266	10.678	10.6134(1)	10.676	10.6611(1)	10.70
Nd–O1 × 6	2.5691	2.5914					
Nd–O2 × 2	2.3064	2.3224					
Zr-O1	2.0939	2.1056					
Nd-Zr	3.7663	3.7924					
x	0.3359	0.3353				0.3357(2)	

Table 3. Frequencies (cm^{-1}) and types of phonon modes at the Γ point. The abbreviations in the "R" (Raman) and "IR" columns: "A" is an active mode, "I" is inactive one. In the last column, the "S" index designates a strong shift ("Strong"), "W" – weak ("Weak").

Type	IR	R	Calc. PBE-SOL0	Calc. PBE0	Exp. [11]	Exp. [10]	Exp. [14]	Exp. [9]	Ions-participants
F_{2u}	I	I	60	51					Nd^S
E_u	I	I	97	93					Nd^S, Zr^W, $O1^W$
F_{1u}	A	I	102	98					Nd, Zr, $O1^W$, $O2^W$
F_{2u}	I	I	134	130					Zr^S, $O1^W$
F_{1u}	A	I	136	131					Nd, $O1^W$, O2
E_u	I	I	138	133					Nd^W, Zr^W, $O1^S$
F_{1u}	A	I	202	199				215	Zr, O1
F_{1u}	A	I	238	234					$O1^S$, $O2^W$
A_{2u}	I	I	249	242					Nd, O1
F_{1g}	I	I	262	253					$O1^S$
F_{2u}	I	I	295	287					$O1^S$
A_{2u}	I	I	309	305					Zr
F_{2g}	I	A	319	309	305	302	298		Nd^S
E_g	I	A	338	328					$O1^S$
F_{1u}	A	I	345	333				365	Zr^W, $O1^W$, O2
A_{2u}	I	I	394	392					O1
F_{1u}	A	I	402	391				400	$O1^W$, $O2^S$
E_u	I	I	410	402					Zr^W, O1
F_{2g}	I	A	422	414	399	400	392		O1, O2
A_{1g}	I	A	518	511	506	501	503		O1
F_{1u}	A	I	522	512				525	O1, $O2^W$
F_{2g}	I	A	546	537	523	516			O1, $O2^S$
F_{1g}	I	I	587	573					O1
F_{2u}	I	I	592	578					O1
F_{2g}	I	A	782	771					O1

Table 4. Frequencies (cm^{-1}) and intensities of IR modes (km/mol). PBE0 calculation.

Type	Frequency	Intensity
F_{1u}	98	316
F_{1u}	131	1992
F_{1u}	199	6504
F_{1u}	234	32
F_{1u}	333	14933
F_{1u}	391	588
F_{1u}	512	3173

Table 5. Raman mode intensity for polycrystalline sample of $Nd_2Zr_2O_7$ (relative units). The intensity of the Raman modes was calculated for $\lambda = 514$ nm and $T = 300$ K. PBE0 calculation.

Type	Frequency, cm^{-1}	I_{tot}	I_{par}	I_{perp}
F_{2g}	309	1000	571	429
E_g	328	205	117	88
F_{2g}	414	27	15	12
A_{1g}	511	54	54	0
F_{2g}	537	69	40	29
F_{2g}	771	25	14	11

Table 6. Raman mode intensity for a single crystal $Nd_2Zr_2O_7$ (relative units). The intensity of the Raman modes was calculated for $\lambda = 514$ nm and $T = 300$ K. PBE0 calculation.

Type	Frequency, cm^{-1}	I_{xx}	I_{xy}	I_{xz}	I_{yy}	I_{yz}	I_{zz}
F_{2g}	309	0	1000	1000	0	1000	0
E_g	328	410	0	0	410	0	410
F_{2g}	414	0	27	27	0	27	0
A_{1g}	511	75	0	0	75	0	75
F_{2g}	537	0	69	69	0	69	0
F_{2g}	771	0	25	25	0	25	0

Table 7. The calculated and experimental Raman modes of the $Nd_2Zr_2O_7$ crystal. Frequencies are given in cm^{-1}. Types of modes are given according to the calculations. The calculated intensities (arb. un.) of the Raman modes for the polycrystalline sample are given in brackets.

Type	Frequency, cm^{-1}	Exp. [10]	Exp. [11]	Notes
F_{2g}	309(1000)	302	305	Zr-O6 bending [11]
E_g	328(205)			
F_{2g}	414(27)	400	399	O-Nd-O′ vib. [10]
A_{1g}	511(54)	501	506	
F_{2g}	537(69)	516	523	
F_{2g}	771(25)		594	

Table 8. Elastic constants and bulk modulus of $Nd_2Zr_2O_7$ (GPa). PBESOL0 calculation.

C_{11}	C_{12}	C_{44}	B
318.8	122.3	102.3	187.8

Table 9. Elastic constants and bulk modulus of $Nd_2Zr_2O_7$ (GPa) at hydrostatic pressure $P = 2$ GPa. PBESOL0 calculation.

C_{11}	C_{12}	C_{44}	B
327.3	128.1	105.5	194.5

Table 10. Bulk modulus, Young's and shear modulus of $Nd_2Zr_2O_7$, GPa. PBESOL0 calculation.

Averaging scheme	Bulk modulus	Young's modulus	Shear modulus	Poisson's ratio
Voigt	187.8	256.2	100.7	0.27
Reuss	187.8	256.1	100.6	0.27
Hill	187.8	256.2	100.7	0.27
Exp. [13]	184	260	103	0.27

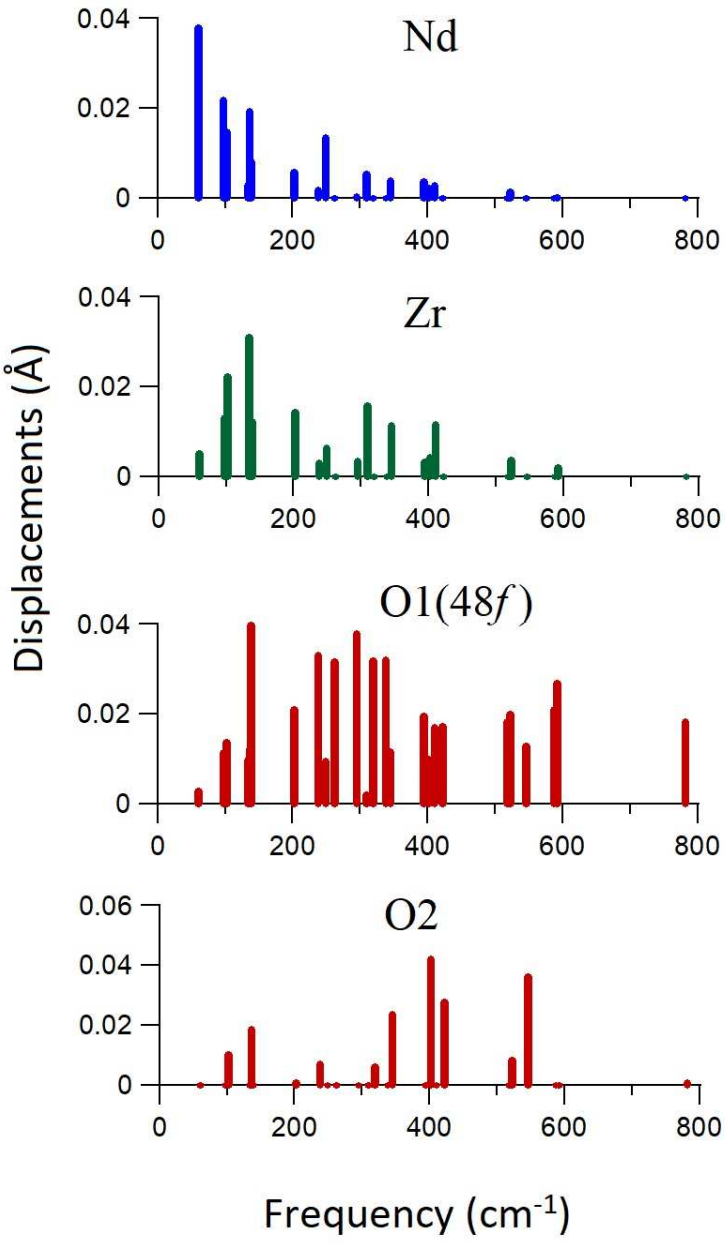

Figure 1. The displacements of ions at phonon modes.

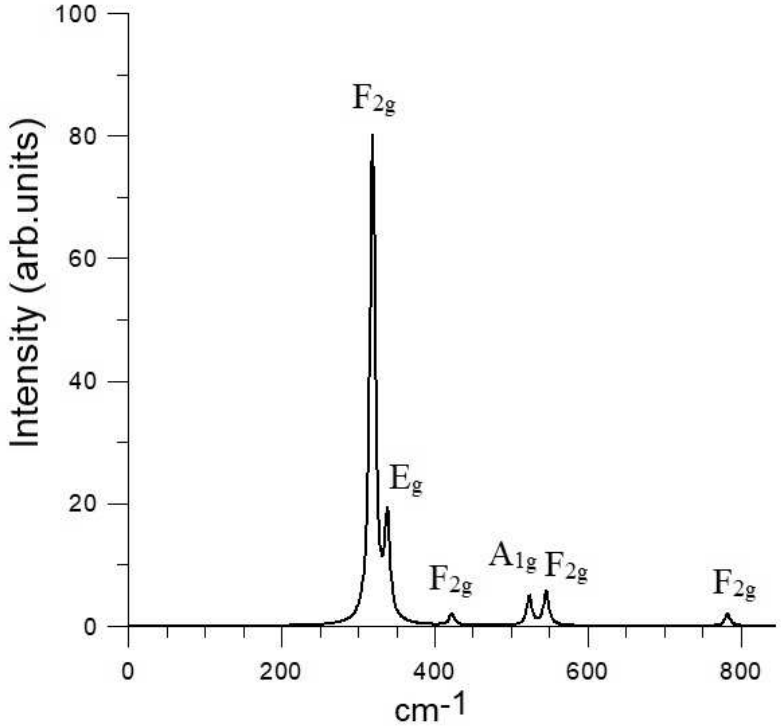

Figure 2. Calculation results of the Raman spectrum of $Nd_2Zr_2O_7$ crystal (PBESOL0 calculation). The intensity of the Raman modes was calculated for $\lambda = 488$ nm and $T = 298$ K. Pseudo-Voigt functions with a damping factor of 8 cm^{-1} were used for modeling of the Raman spectrum based on the calculated frequencies and intensities for a polycrystal.

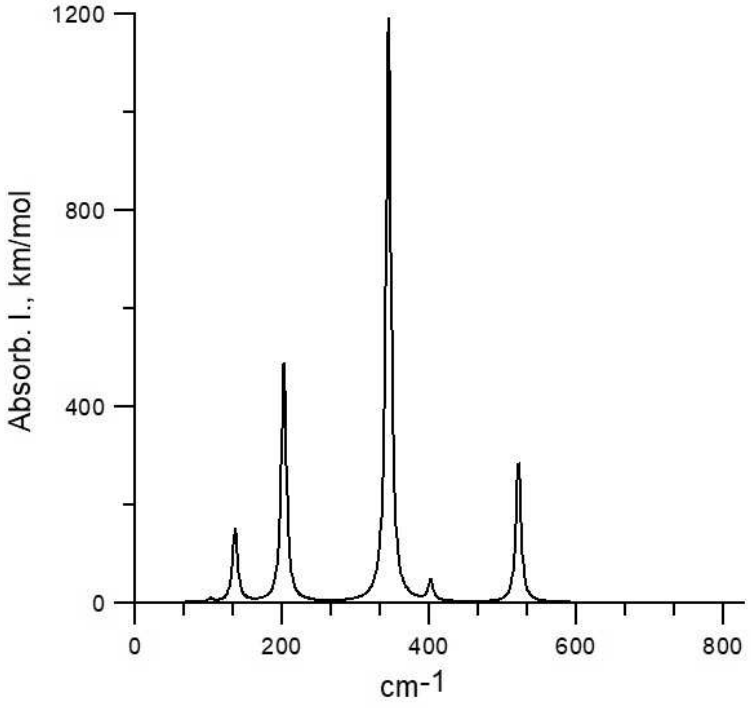

Figure 3. Calculation results of the IR spectrum of $Nd_2Zr_2O_7$ (PBESOL0 calculation). All infrared modes are of F_{1u} type.

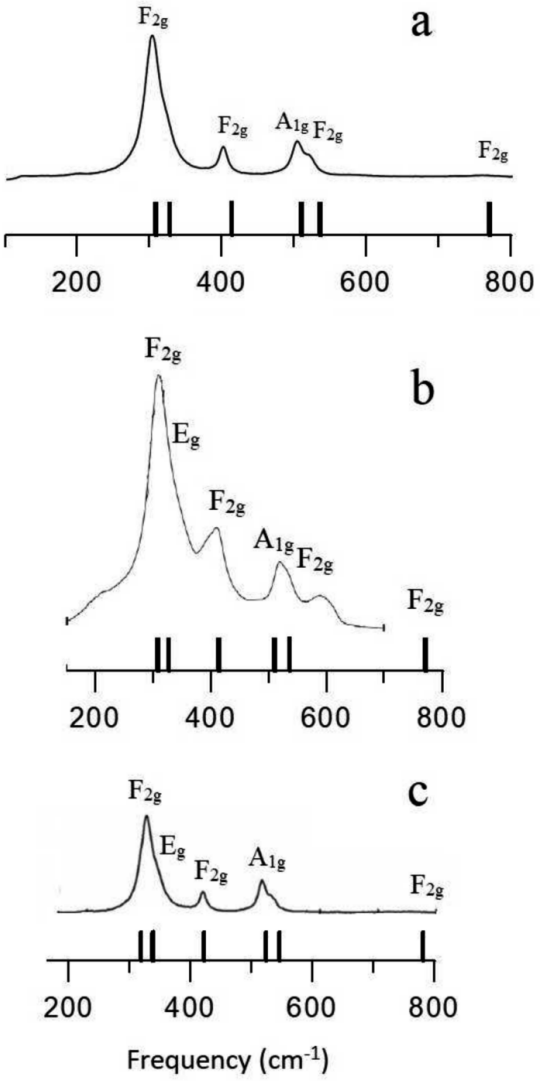

Figure 4. The calculated and experimental Raman modes of the $Nd_2Zr_2O_7$ crystal. The calculated frequencies are indicated by vertical bars. Types of modes are given according to the calculations. PBE0 calculations are presented in (a) and (b). PBESOL0 calculation is shown in (c). The experimental data [10], [11], [12] are presented in (a), (b) and (c), respectively.

4. Summary

Ab initio calculation of the crystal structure and phonon spectrum $Nd_2Zr_2O_7$ with the pyrochlore structure are carried out within the framework of the MO LCAO approach with a hybrid DFT functionals that takes into account the contribution of the HF exchange. The calculations reproduce the crystal structure in good agreement with the experimental data. Based on the analysis of displacement vectors obtained from these *ab initio* calculations, the degree of participation of each ion in a particular mode is estimated. It is shown that only oxygen ions are involved in Raman modes. The modes with absolute or predominant participation of oxygen at the 48*f* position, characterized by the displacement textitx, are determined. The obtained results can be used for interpretation of the Raman and IR spectra of the crystal.

Acknowledgments

This study was supported by the Ministry of Education and Science of the Russian Federation (project No. 3.9534.2017/8.9).

References

1. Hatnean M.C., Decorse C., Lees M.R., Petrenko O.A., Balakrishnan G. *Crystals* **6**, 79 (2016)
2. Hatnean M., Lees M.R., Petrenko O.A., Keeble D.S., Balakrishnan G., Gutmann M.J., Klekovkina V.V., Malkin B.Z. *Phys. Rev. B* **91**, 174416 (2015)
3. Tao F., David C., Danyu J., Jinfeng X., Jianlin S. *Appl. Phys. Lett.* **98**, 151105 (2011)
4. Malkin B.Z, Lummen T.T., van Loosdrecht P.H., Dhalenne G., Zakirov A.R. *J. Phys. Cond. Mat.* **22**, 276003 (2010)
5. Xu J., Anand V.K., Bera A.K., Frontzek M., Abernathy D., Casati N., Siemensmeyer K., Lake B. *Phys. Rev. B* **92**, 224430 (2015)
6. Popov V.V., Menushenkov A., Gaynanov B.R., Zubavichus Y.V., Svetogorov R.D., Yastrebtsev A.A., Pisarev A.A., Arzhatkina L.A., Ponkratov K.V. *J. Phys.: Conf. Ser.* **941**, 012079 (2017)
7. Shimamura K., Arima T., Idemitsu K., Inagaki Y. *Int. J. Thermophysics* **28**, 1074 (2007)
8. Subramanian M., Aravamudan G., Rao G.S. *Progr. Sol. St. Chem.* **15**, 55 (1983)
9. Klee W.E., Weitz G. *J. Inorg. Nucl. Chem.* **31**, 2367 (1969)
10. Kong L., Karatchevtseva I., Gregg D.J., Blackford M.G., Holmes R., Triani G. *J. Eur. Ceramic Soc.* **33**, 3273 (2013)
11. Banerji A., Mandal B.P., Sairam T.N., Tyagi A.K. *Sol. State Comm.* **151**, 321 (2011)
12. Sattonnay G., Sellami N., Thome L., Legros C., Grygiel C., Monnet I., Jagielski J., Jozwik-Biala I., Simon P. *Acta Materialia* **61**, 6492 (2013)
13. Shimamura K., Arima T., Idemitsu K., Inagak Y. *Int. J. Thermophys.* **28**, 1074 (2007)
14. Kaliyaperumal C., Sankarakumar A., Palanisamy J., Paramasivam T. *Materials Lett.* **228**, 493 (2018)
15. Mustafa G.M., Saleem M., Atiq S., Riaz S., Saadat A., Siddiqi S.A., Naseem S. *J. Saudi Chem. Soc.* **23**, 397 (2019)
16. Gupta S., Sudarshan K., Ghosh P.S., Srivastava A.P., Bevara S., Pujari P.K., Kadam R.M. *J. Mater. Chem. C* **4**, 4988 (2016)
17. Perdew J.P., Ernzerhof M., Burke K. *J. Chem. Phys.* **105**, 9982 (1996)
18. Dovesi R., Saunders V.R., Roetti C., Orlando R., Zicovich-Wilson C.M., Pascale F., Civalleri B., Doll K., Harrison N.M., Bush I.J., D'Arco P., Llunel M., Causa M., Noel Y., Erba A., Casassa S. *CRYSTAL17. User's Manual* (2018) `http://www.crystal.unito.it/Manuals/crystal17.pdf`
19. Dovesi R., Erba A., Orlando R., Zicovich-Wilson C.M., Civalleri B., Maschio L., Rerat M., Casassa S., Baima J., Salustro S., Kirtman B. *Comp. Mol. Sci.* **8**, e1360 (2018)
20. Evarestov R.A., Bandura A.V., Aleksandrov V.E. *Phys. Sol. St.* **47**, 2248 (2005)
21. Medvedev M.G., Bushmarinov I.S., Sun J., Perdew J.P., Lyssenko K.A. *Phys. Sol. St.* **355**, 49 (2017)
22. Chernyshev V.A., Petrov V.P., Nikiforov A.E., Agzamova P.A., Avram N.M. *Opt. Mater.* **72**, 565 (2017)
23. Peintinger M.F. Oliveira D.V., Bredow T. *J. Comp. Chem.* **34**, 451 (2012)

24. *CRYSTAL website:* `http://www.crystal.unito.it/index.php`
25. Valenzano L., Civalleri B., Chavan S., Bordiga S., Nilsen M., Jakobsen S., Lillerud K.P., Lamberti C. *Chem. Mater.* **23**, 1700 (2011)
26. Dolg M., Stoll H., Savin A., Preuss H. *Theor. Chim. Acta* **75**, 173 (1989)
27. Dolg M., Stoll H., Preuss H. *Chem. Mater.* **85**, 441 (1993)
28. Yang J., Dolg M. *Theor. Chem. Acc.* **113**, 212 (2005)
29. Weigand A., Cao X.,Yang J., Dolg M. *Theor. Chem. Acc.* **126**, 117 (2009)
30. `http://www.tc.uni`
31. Maschio L., Kirtman B., Orlando R., Rerat M. *J. Chem. Phys.* **137**, 204113 (2012)
32. Maschio L., Kirtman B., Rerat M., Orlando R., Dovesi R. *J. Chem. Phys.* **139**, 164101 (2013)
33. Maschio L., Kirtman B., Rerat M., Orlando R., Dovesi R. *J. Chem. Phys.* **139**, 164102 (2013)
34. Orlando R., Lacivita V., Bast R., Ruud K. *J. Chem. Phys.* **132**, 244106 (2010)
35. Dovesi R., Orlando R., Erba A., Zicovich-Wilson C.M., Civalleri B., Casassa S., Maschio L., Ferrabone M., Pierre M.D.L., D'Arco P., Noel Y., Causa M., Rerat M., Kirtman B. *Int. J. Quant. Chem.* **114**, 1287 (2014)
36. Prosandeev S., Waghmare U., Levin I., Maslar J. *Phys. Rev. B* **71**, 214307 (2005)
37. Wu Z., Zhao E., Xiang H., Hao X., Liu X., Meng J. *Phys. Rev. B* **76**, 054115 (2007)